WAVE OVERTOPPING AT VERTICAL WALLS IN SHALLOW WATER CONDITIONS: A PREDICTIVE FORMULA

Sara Tuozzo[1], Mario Calabrese[1] and Mariano Buccino[1]

The work examines the wave overtopping process of vertical seawalls with very shallow foreshores. The non-hydrostatic model SWASH is used as an exploratory tool to deepen our knowledge about this process. Nowadays, phase-resolving numerical models are indeed considered reliable tools due to their attested ability to capture the physics of complex hydrodynamics phenomena, such as wave overtopping. Specifically, we explore the relationship between the mean overtopping discharge and the Fourier power spectrum, and then we provide a new overtopping model. The latter relates the flow rate to a new time-domain statistic representing the upper tail of wave elevation distribution at the toe of the structure. Finally, almost 200 laboratory experiments validate numerical findings.

Keywords: wave overtopping; seawalls; shallow foreshores; numerical analysis

INTRODUCTION

Wave overtopping is one of the wave-structure interaction phenomena that has largely fascinated coastal engineering and scientific communities, as demonstrated by the large body of literature that is still dealing with it.

Engineers usually quantify the overtopping risk through specific variables, such as the mean overtopping discharge, the individual maximum overtopping volume, or the flow's thickness and velocity. Among them, the mean rate q is still considered a key parameter for coastal flood risk assessment and sea defenses design, even though it cannot account for the inherent complexity of this process due to its stochastic and temporally variable nature. Different kinds of tools allow us to estimate q, including physical/numerical modelling (Buccino et al., 2023; Di Leo et al. 2022; Altomare et al., 2021; Suzuki et al., 2017; Losada et al., 2008) or empirically-based instruments, such as machine learning techniques (den Bieman et al., 2021; Zanuttigh et al., 2016) and regression formulae (e.g. EurOtop, 2018). In this work, we focus on the latter since they can take into account the physics of the process and simultaneously exploit data information.

Empirical formulae for wave overtopping may be distinguished according to the hydraulic variables adopted. Indeed, several authors use a run-up level since the overtopping essentially occurs when the run-up height exceeds the crest freeboard of the structure (Etemad-Shahidi et al., 2022; Yuhi et al., 2021 Hedge and Reis, 1998); on the other hand, wave conditions – measured in deep water or at the toe of the structure – are frequently employed (Lashley et al., 2021; EurOtop, 2018). However, the first group of overtopping model is characterized by the uncertainties related to the estimation of the run-up itself. The second group, instead, might be affected by the challenging estimation of wave parameters in very shallow water conditions or, in the case of deep-water-based-models, by the difficult of extending the formula to sea defenses fronted by complex bathymetries (Lashley et al., 2023).

The present work addresses the overtopping of vertical seawalls with very shallow foreshores. Indeed, although these sea defense solutions are being widely adopted to protect coastal zones from flooding, Buccino et al. (2023) have highlighted the paucity of existing reliable data, which thus questions the validity of the overtopping predictive formulae. Furthermore, the lack of information sheds some doubts on the effective relationship between mean overtopping discharge and harmonic spectral period, T_{m-10}, which is anything but easy to estimate in case of very shallow water and heavy breaking. According to Buccino et al., T_{m-10} indeed affects q just because of a spurious correlation effect.

Therefore, we first aim to deepen the relationship between mean overtopping discharge and the Fourier power spectrum, and, then, to derive a robust overtopping predictive equation for vertical walls in shallow water conditions. To achieve these objectives, we employ the non-hydrostatic model SWASH. Finally, numerical findings are verified with almost 200 laboratory experiments.

NUMERICAL EXPERIMENTAL CAMPAIGN

The experimental campaign has been carried out via the numerical model SWASH (Zjilema et al., 2011). Numerical investigation indeed allows us to avoid the typical constraints of physical experiments and vary as much as possible the hydraulic and geometrical conditions tested; hence, we have gathered a wide and varied dataset. The latter is composed by two distinct groups: the former inspects the hydraulic variables that better explain the overtopping process; while the second one addresses the development of a new empirical formula.

[1] University of Naples Federico II, Italy. sara.tuozzo@unina.it

Numerical model SWASH

SWASH is a phase-resolving model that integrates the Non-Linear Shallow Water equations extended with a non-hydrostatic pressure term:

$$\frac{\partial \zeta}{\partial t} + \frac{\partial hu}{\partial x} = 0 \qquad (1)$$

$$\frac{\partial u}{\partial t} + u\frac{\partial u}{\partial x} + g\frac{\partial \zeta}{\partial x} + \frac{1}{2}\frac{\partial p_b}{\partial x} + \frac{1}{2}\frac{p_b}{h}\frac{\partial(\zeta - d)}{\partial x} + c_f \frac{u|u|}{h} = 0 \quad (2)$$

$$\frac{\partial \omega_s}{\partial t} = \frac{2p_b}{h} - \frac{\partial\, \omega_b}{\partial t}, \omega_b = -u\frac{\partial d}{\partial x} \quad (3)$$

$$\frac{\partial u}{\partial x} + \frac{\omega_s - \omega_b}{h} = 0 \quad (4)$$

where u is the depth-averaged velocity in x-direction, ω_s and ω_b are the velocities in z-direction at the free surface and at the bottom respectively, ζ is the free surface elevation from the still water level, d is the still water depth and h the total depth, p_b is the non-hydrostatic pressure at the bottom, g is the gravitational acceleration and c_f is the dimensionless bottom friction coefficient.

Eqs. (1, 2) are the conservation of mass and momentum for a depth-averaged, non-hydrostatic, free-surface flow; while Eqs. (3, 4) are the momentum equation for the vertical velocity at free surface, along with the kinematic boundary condition for vertical velocity at the bottom, and the local mass continuity, respectively (see Zijlema et al., 2011). The addition of the two extra equations and the Keller box scheme (Lam and Simpson, 1976) ensures that the non-hydrostatic pressure is accounted for. Moreover, the single-valued representation of the free surface in the horizontal plane, $\zeta(x,y,t)$, avoids requiring additional free surface treatment methods.

The dispersive properties of the model can be enhanced by resorting to a multi-layer mode, i.e. the domain is vertically divided into a fixed number of layers. However, using the Keller Box scheme to handle the pressure gradients in the vertical momentum equation guarantees good dispersive properties even at low vertical resolution. Contemporary, the Hydrostatic Front Approximation (HFA) developed by Smit et al. (2013) allows an appropriate reproduction of wave breaking even with few layers. It is worth specifying that SWASH adopts the shock capturing scheme to reproduce the energy dissipation.

Finally, the system of equation, Eqs. (1 - 4), is completed by imposing boundary conditions at the open boundaries of the computational domain. At the offshore edge, waves are generated by prescribing the horizontal particle velocities normal to the boundary over the vertical. In addition, a weakly reflective condition avoids some reflections. Either periodic or random waves can be generated. The latter could have a specific parametric shape (e.g. JONSWAP); moreover, it can be modified by adding a second-order correction term that allows to generate bound IG-waves (Rijnsdorp et al., 2014). At the onshore boundary, either a Sommerfeld's radiation condition or a sponge layer can be applied to prevent wave reflection.

The numerical scheme consists of an explicit, second order accurate finite difference method for staggered grid that conserves both mass and momentum at the numerical level, and a second-order leapfrog scheme for time integration, with an adaptive time step that satisfies the Courant-Friedrichs-Lewy stability condition.

Numerical experimental campaign

As mentioned above, two types of experiments have been performed to achieve the objectives of this work. The first allows us to empirically verify the effective role of the hydraulic variables in the estimation of the mean overtopping discharge (such tests will be referred as *HV* hereafter); based on the *HV*' findings, the second group of experiments (referred as *OF* hereafter) avails us to develop a new predictive formula.

HV experiments include 34 tests comparing the behavior of random and periodic wave trains and eight random wave tests that differ in the spectral moments at the toe of the walls. The former group has been conducted on a planar beach inclined 1/10 to the horizontal (Fig. 1a) and considers two crest freeboards, R_C, and a fixed value of water depth at the toe of the structure, h_{TOE} (Table 1). Analogously,

the second group has been run with two different values of R_C and a fixed value of h_{TOE}; however, the bathymetry is characterized by a multi-slope profile (Fig. 1b). Moreover, these 8 tests resort to both the linear and second-order generation theories mentioned in the previous Section. Specifically, the random waves are ruled by the mean JONSWAP spectrum.

The second experimental phase concerns 74 *OF* tests, which have been carried out on planar beaches with different slopes (Fig. 1c). In particular, we have considered a steeper beach inclined 1 to 10 to the horizontal, and two mild slopes (*tan(m)* = 1/30 and 1/50). Furthermore, the water depth at the toe of the structures has been varied in order to examine different shallowness conditions (from shallow to extremely shallow water); indeed, according to the classification of Hofland et al. (2017), $h_{TOE}/H_{m0,deep}$ varies between 2.7 and 0.2. The crest freeboard has been varied as well. Wave conditions are characterized by a deepwater wave steepness equal to 0.035, which is a typical value of sea waves. Random wave trains are driven by mean JONSWAP wave spectra; the linear generation theory has been adopted.

Table 1 reports the details of the *OF* experiments. It is worth pointing out that we have performed separately wave propagation tests and wave overtopping tests. Thus, we have obtained the incident wave conditions without the presence of the structure in the numerical flume. Wave propagation simulations run for 200 waves, while overtopping tests run for 500 waves (according to the findings of Romano et al., 2015).

Table 1. Main features of the numerical experiments.

	# tests	wave generation	slope type	h_{TOE} [m]	$H_{m0,deep}$ [m]	$T_{p,deep}$ [s]	R_C [m]
HV	34	random/periodic	Planar	1	1.4 ÷ 6.4	5 ÷ 12	1; 2
HV	8	random	Uneven	3.43	5.9 ÷ 8.2	12	2.2; 4.4
OF	74	random	Planar	0.6 ÷ 14.4	1.3 ÷ 5.3	5.3 ÷ 10	0.4 ÷ 5.8

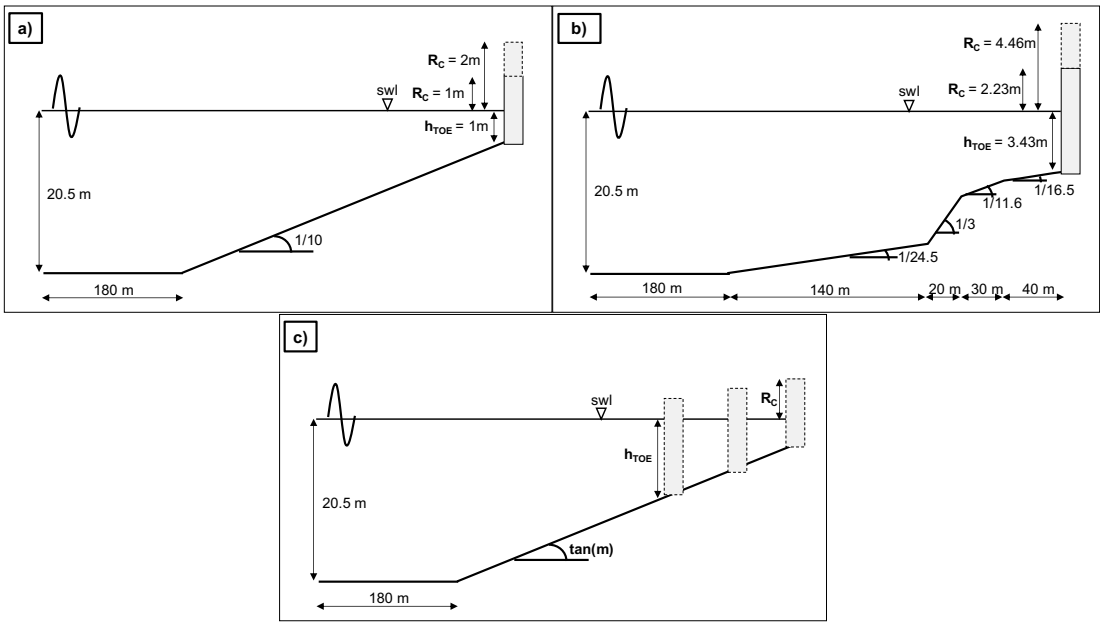

Figure 1. Sketch of the geometrical features adopted during the numerical experimentation. Panel a) and b) refer to the *HV* tests, while panel c) refers to the *OF* tests.

Numerical setup

The numerical experiments have been conducted in a 1-D mode using the non-hydrostatic correction.

At both the edges of the numerical flume, a weakly reflective boundary condition has been imposed. Concerning the spatial discretization, 2 vertical layers have been adopted, while the grid spacing varies according to the wave conditions tested. In particular, it guarantees at least the ratio $\Delta x/L_{nb} = 70$, where L_{nb} represents somehow the nominal wavelength at the incipient breaking (i.e., $L_{nb} = (g \cdot H_{m0,deep})^{0.5}$). The maximum Courant number has been assigned equal to 0.5.

The wave breaking has been modelled via the HFA approach, using the default values (i.e. $\alpha = 0.6$, $\beta = 0.3$). A zero value of the Manning coefficient has been adopted.

NUMERICAL RESULTS

HV experiments

In this Section, we aim to empirically verify the findings of Buccino et al. (2023), which stated that the influence of the harmonic spectral period on the mean overtopping discharge is due to a spurious correlation effect. However, the authors achieved this conclusion based on merely statistical analysis; thus, we have tried to find more direct evidence. Moreover, Buccino et al. introduced a new water level statistic, $\zeta_{1/4}$, to predict q; hence, *HV* tests try to corroborate the explanatory power of this new hydraulic variable.

For the 8 random wave tests conducted on the uneven profile (Fig.1b), we exploit two wave generation boundary conditions to obtain wave spectra at the toe of the walls that differ solely in terms of wave energy at low-frequency components – the same values of m_0 and f_p but different m_{-1} (i.e. different $T_{m-10,TOE}$). Indeed, previous investigations (not shown here for the sake of brevity) pointed out that the first- and second-order generation theories can lead to different evolution for surf beats, even though the generated spectra have the same energy and approximately the same shape. Conversely to the literature statement (e.g., see Eqs.7.7,7.8 of the EurOtop Manual), numerical outcomes show that the larger mean overtopping discharge has been obtained with the lower value of the harmonic spectral period (Fig.2a). Nevertheless, we can observe that – for a given wave energy – the greater value of flow rate is related to the higher wave set-up reached at the toe of the structure (Fig.2b). Hence, quantities such as wave setup and wave skewness, which are inherently not reflected in the spectrum, might have a crucial role in the overtopping process. Fig.2 suggests that the mean flow rate depends on the water level at the toe of the structure, which can be expressed by new statistic introduced by Buccino et al. (2023); indeed, the average of the highest one-fourth of wave elevation, $\zeta_{1/4}$, represents the tail with low exceedance probability of the $\zeta(t)$ statistical distribution.

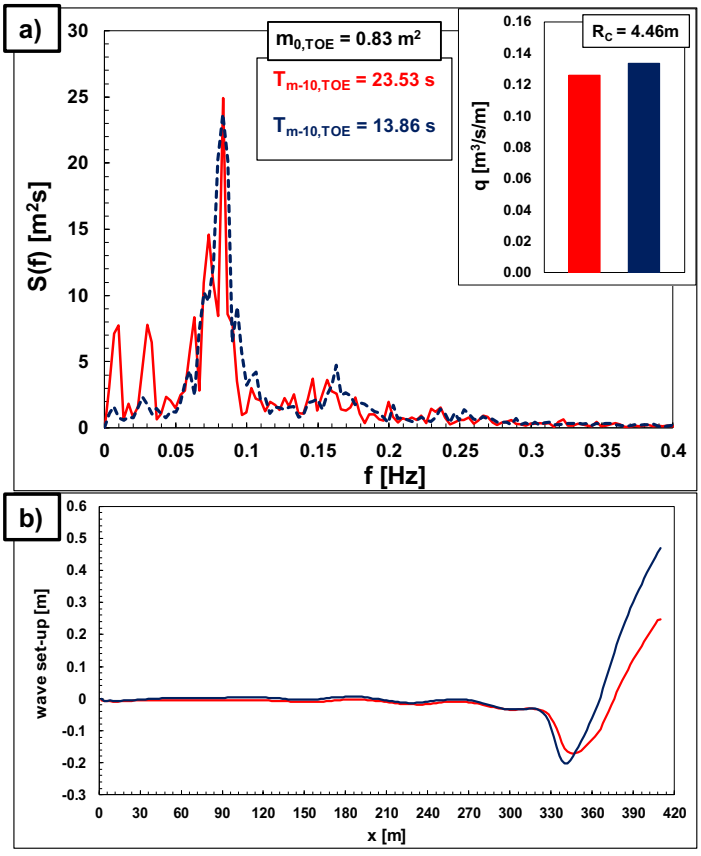

Figure 2. Comparison between the mean overtopping discharge of two incident waves characterized by the same total wave energy, but different harmonic spectral period (panel a) and wave set-up (panel b) at the toe of the wall.

Overall, the previous findings establish that the mean overtopping discharge is affected by the wave elevation distribution instead of the spectral distribution of wave energy. To further corroborate such assessment, we compare the behavior of random and periodic wave trains as they experience dramatic differences in the spectral shapes (Figs.3a,b). Furthermore, periodic waves do not exhibit wave energy at low-frequencies. As shown in Fig.3c, $\zeta_{1/4}$ ensures that, for each crest freeboard tested, the flow rates of random and periodic waves remarkably follow a unique trend, confirming the crucial role of the new variable. Indeed, for a given value of $\zeta_{1/4}$ and R_C, periodic and random sea states provide a similar discharge (the data circled in blue in Fig.3c) despite the significant difference in the energy spectral distribution (Figs.3a,b).

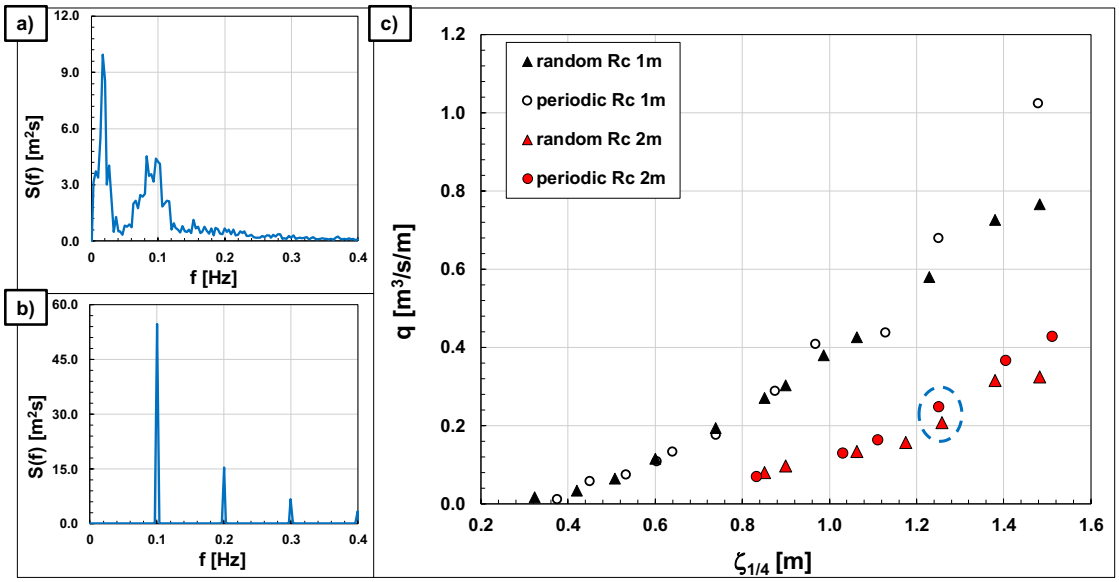

Figure 3. Mean overtopping discharge of random and periodic wave trains. Panels a) and b) compares the wave energy spectra of random and periodic wave trains, respectively; panel c) depicts *q* as a function of the highest one-fourth of wave elevation at the toe of the wall. The two points circled in panel c) refer to the wave spectra of panels a) and b).

Nevertheless, these findings do not indicate that surf beats have no rule in the overtopping process. Based on our analysis, we simply assess that low- and short-frequency components have the same weight in estimating the mean overtopping discharge.

OF experiments

Based on the previous results, we aim to exploit the novel time-domain statistic developing a new overtopping predictive tool. The interesting property of $\zeta_{1/4}$ is that, either for a Gaussian wave process or sinewave trains, it can be determined through two phase-averaged quantities:

$$\zeta_{1/4} = \mu + 1.27\sqrt{m_{0,TOE}} \qquad (1)$$

where indeed μ is the wave set-up (or wave set-down). Unlike the results of Fig.3 that refer to the measured $\zeta_{1/4}$, in the following analysis we will estimate it via Eq. 1. It is worth noting that the latter neglects the effect of wave skewness.

Overall, the second experimental phase consists in a wide parametric study that allows us to establish the variables involved in the overtopping process of vertical walls with shallow foreshores and, thus, develop a new predictive formula.

According to the numerical findings, we propose a new parametrization for estimating the dimensionless overtopping discharge. Specifically, we develop two hypotheses of parametrization: the first is more theoretically consistent, whereas the second one leans on empirical observations. Clearly, the dimensionless freeboard is obtained using the new hydraulic variable (Eq. 1).

- The hypothesis 1 of parametrization reads:

$$\frac{q}{g \cdot H_{m0}^{*} \cdot T_{p,deep}} = F\left(\frac{R_C}{\zeta_{1/4}} \cdot \gamma_{br} \right) \quad (2)$$

where H_{m0}^{*} at the left-hand side of Eq. 2 is:

$$H_{m0}^{*} = \min\left\{ H_{m0,deep}; h_{TOE} \cdot \left[\gamma_0 \exp\left(p \cdot \tan(m) \right) \right] \right\} \quad (3)$$

while the coefficient γ_{br} is:

$$\gamma_{br} = \max\left\{ 1; \frac{h_{TOE}}{H_{m0,deep}} \cdot \tanh\left(8 \cdot \pi \cdot \frac{h_{TOE}}{L_{p,deep}} \right) \right\}^{0.33} \quad (4)$$

In Eq. 2, we obtain the dimensionless discharge using the significant wave height and the deep water peak period, recalling the Owen (1980) overtopping model. Furthermore, in the case of breaking waves, the significant wave height is determined using a sort of Kamphuis model (1991) (Eq. 3). Specifically, Eq. 3 allows us to directly take into account the role of the foreshore slope in very shallow waters.

The coefficient γ_{br} at the right-hand side of Eq. 2, recalls the term used in the studies on the nature of loading at monolithic structures (e.g., Calabrese and Buccino, 2000, Vicinanza et al., 2015) to distinguish between impulsive and pulsating waves (Eq. 4). In particular, γ_{br} amplifies the relative crest freeboard for seawalls located towards deep water (waves tending to pulsating conditions) to compensate for the lower flow rate of the non-impulsive waves.

- On the other hand, the hypothesis 2 of parametrization is:

$$\frac{q}{g \cdot h_{TOE} \cdot T_{p,deep} \cdot \tan(m)^{P}} = F'\left(\frac{R_C}{\zeta_{1/4}} \cdot \gamma'_{br} \right) \quad (5)$$

in which P and γ'_{br} has the following expression, respectively:

$$P = \frac{0.5}{\left[1 + 50 \cdot \exp\left(-10 \cdot \frac{H_{m0,deep}}{h_{TOE}} \right) \right]} \quad (6)$$

$$\gamma'_{br} = \max\left\{ 1; \frac{h_{TOE}}{H_{m0,deep}} \cdot \tanh\left(10 \cdot \pi \cdot \frac{h_{TOE}}{L_{p,deep}} \right) \right\} \quad (7)$$

where Eq. 6 expresses the seaward diminishing influence of the foreshore slope on the overtopping process, while – analogously to Eq. 4 – Eq. 7 amplifies the relative crest freeboard of walls with shallow foreshores. Moreover, due to the difference in the dimensionless q between Eqs. 2 and 5, γ'_{br} has the additional role of empirically compensating for the artificial reduction of the dimensionless flow rate caused by the increase of h_{TOE} for deep water structures.

Overall, beyond the specific features of the two hypotheses, the structure of the proposed parametrization ensures the estimation of the flow rate in a wide range of shallowness conditions; indeed, the predictive tool provided below can be used for both breaking and non-breaking waves.

Fig. 4 plots the numerical outcomes of the *OF* experiments according to the dimensionless variables of Eqs. 2 and 5. The data are distinguished based on the shallowness conditions. For both the hypothesis of parametrization, a double-power function fits the numerical data; the fitting coefficients are reported in Figs.4a and 4b for the first and second hypotheses, respectively. Further details can be found in Tuozzo et al. (2024).

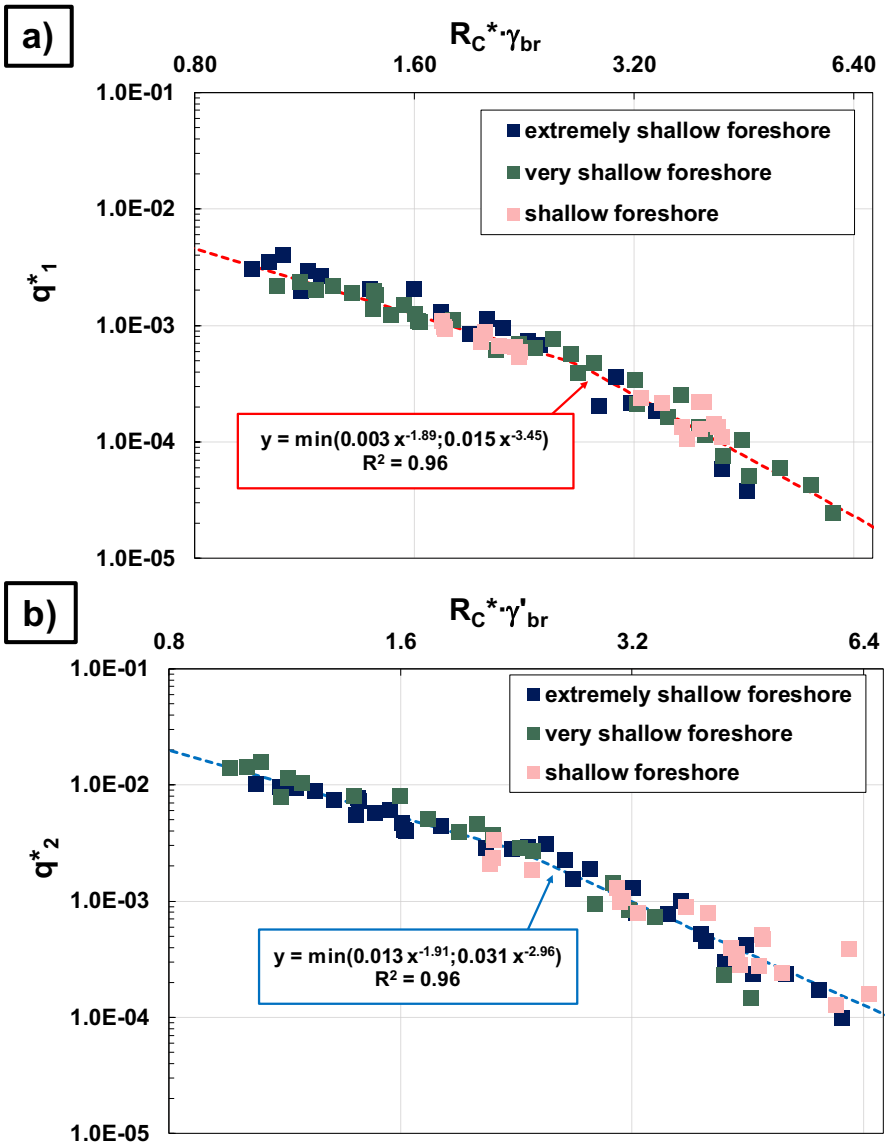

Figure 4. *OF* numerical data plotted according to the new parametrization. Panel a) refers to the first hypothesis (Eqs. 2 – 4), while panel b) refers to the second one (Eqs. 5 – 7).

NEW PREDICTIVE FORMULA

Finally, we aim to evaluate the new parametrization's performance in extended shallowness conditions and provide a more generalized formula for estimating the wave overtopping of seawalls in shallow water. Thus, we verify the previous results with almost 200 laboratory tests.

Specifically, we have gathered two main datasets:

- EurOtop reliable data (RF=1 and 2, according to the Manual classification);
- experiments conducted at the University of Naples Federico II on the Malecòn multi-slope profile (Cordova Lopez et al., 2016).

The former dataset encompasses 146 data of vertical walls with shallow and very shallow foreshore; moreover, these data include impulsive and pulsating wave conditions. The second dataset contains 48 overtopping data in shallow and very shallow water, which were conducted on an uneven profile (i.e. vertical seawalls fronted by a multi-slope beach). Table 2 summarizes the main features of both these datasets.

Table 2. Main characteristics of laboratory datasets

	# tests	slope type	$h_{TOE}/H_{m0,deep}$ [-]	impulsive conditions
EurOtop (2018) RF=1&2	146	planar	0.82 ÷ 3.9	impulsive/pulsating
Cordova et al. 2016	48	uneven	0.52 ÷ 1.48	impulsive

It is worth specifying that the EurOtop database does not provide information about the mean wave set-up of the laboratory tests. However, to determine the new variable $\zeta_{1/4}$ (Eq. 1), we can reasonably assume a zero value of μ since the lowest value of $h_{TOE}/H_{m0,deep}$ is 0.82 (see Table 2).

On the other hand, we need an equivalent slope representing the uneven bathymetry of Cordova et al.'s data in order to verify our parametrization (see *tan(m)* in Eqs. 3 and 5). According to the findings of Tuozzo et al. (2024), we adopt an equivalent slope that is averaged on twice the local wavelength at the toe of the structure.

For the sake of brevity, in the following we will show the results relative to the hypothesis 2 of parametrization (Eqs. 5-7); however, analogous results have been obtained using (Eqs. 2-4). Hence, Fig. 5 plots laboratory data according to the new dimensionless variables. Moreover, it depicts the empirical formula gathered from numerical data in Fig. 4b as well (referred to as SWASH formula). In particular, it is worth pointing out that the numerical study did not investigate the parametrization's behavior for relative crest freeboards higher than 6; thus, the extrapolated formula is depicted as dash-dotted curves.

As can be appreciated in the Figure, laboratory data confirm the validity of the numerical findings and, thus, the good explanatory power of our parametrization. Both datasets follow indeed a unique trend with a significant reduction in data scattering compared to the EurOtop parametrization, as shown in Fig. 6. Additionally – conversely to the EurOtop model that provides two different predictive formulas – it is worth emphasizing that our parametrization guarantees a unique behavior for both impulsive and pulsating wave loads.

Despite the consistency between numerical findings and laboratory data, the SWASH formula mostly lies below the cloud of data; however, this slight underestimation of the non-hydrostatic model is not unexpected as it has been already observed in literature (see Buccino et al. 2023, Suzuki et al. 2017). Therefore, the coefficients of the double power law have been recalibrating to fit the laboratory data; thus, the new predictive formula for vertical seawalls in shallow waters reads:

$$\frac{q}{g \cdot h_{TOE} \cdot T_{p,deep} \cdot \tan(m)^P} = \min\left[0.0107\left(\frac{R_C}{\zeta_{1/4}} \cdot \gamma'_{br}\right)^{-1.49} ; 0.068\left(\frac{R_C}{\zeta_{1/4}} \cdot \gamma'_{br}\right)^{-3.04} \right] \quad (8)$$

As specified above, Eq. 8 is valid for both breaking and non-breaking waves.

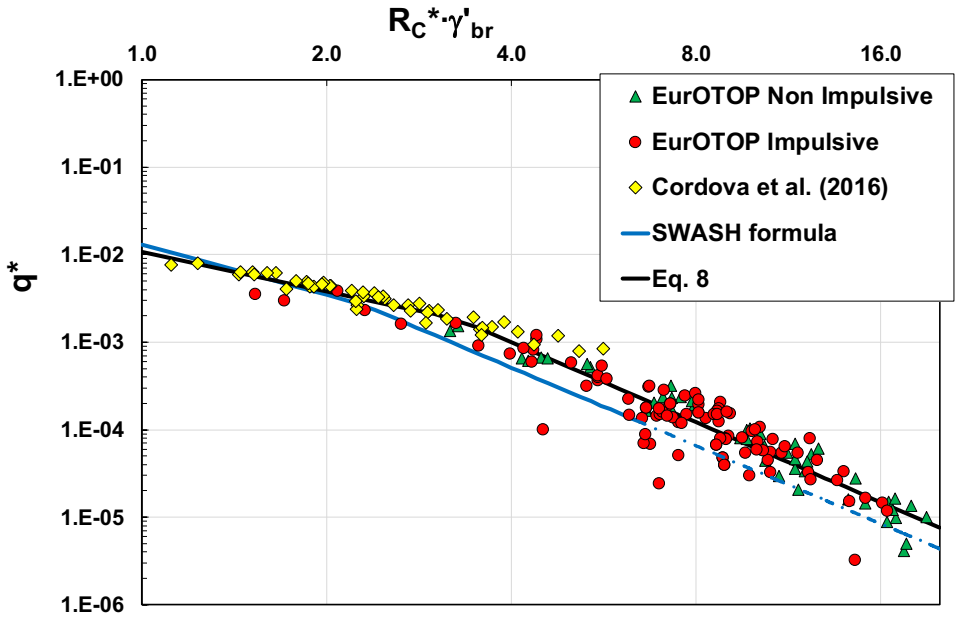

Figure 5. Laboratory datasets plotted according the new parametrization (Eqs. 5-7). The numerical double power law (blue line) and the re-calibrated formula (black line) are plotted as well.

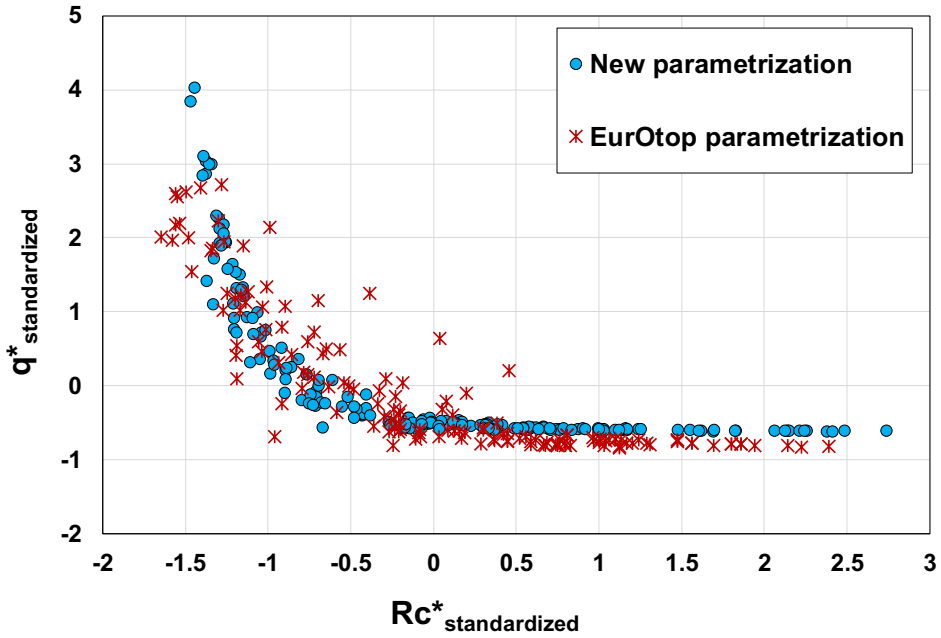

Figure 6. Comparison between the new parametrization (Eqs. 5 – 7) and that one used in the literature (EurOtop, 2018). The red cross points only include impulsive data, as the EurOtop propose two different dimensionless variable depending on the wave loads.

CONCLUSIONS

The present work examines the overtopping at vertical seawalls in shallow water, focusing on the relationship between the mean overtopping discharge and the hydraulic variables involved in the process. The analysis has been carried out using the non-hydrostatic model SWASH as an explorative tool. Indeed, numerical models are nowadays capable of resolving complex physical processes (e.g., Buccino et al., 2021, 2022), allowing to easily vary the experimental conditions smoothly, avoiding the typical limitations (in terms of space and wave variables) of laboratory experiments.

In the first part of the work, we inspect the relationship between q and the Fourier spectrum – widely adopted in the literature – questioning the established role of the harmonic spectral period in the wave-structure interaction processes in shallow water conditions. Starting from the findings of Buccino et al. (2023), which demonstrated through a statistical analysis that T_{m-10} affects q because of a spurious correlation effect, we have tried to provide more empirical proofs via ad hoc numerical experiments. The results of *HV* tests corroborated such a statement, demonstrating that the flow rate is actually governed by the water elevation distribution at the toe of the wall rather than the energy spectral distribution (i.e., T_{m-10}). Specifically, the new time-domain statistic $\zeta_{1/4}$ (i.e., the highest one-fourth of wave elevation distribution at the toe of the wall) appears as an efficient variable for estimating the mean overtopping rate. Actually, it is worth highlighting that the use $\zeta_{1/4}$ is physically consistent with the use of extreme run-up statistics (e.g., $R_{2\%}$) for predicting q, but its estimation is much simpler as it is inferred without the presence of the structure. Furthermore, using this new hydraulic variable emphasizes the crucial role of the mean wave set-up in the overtopping process.

The second phase of the work combines these findings and a wide parametric study (namely, the *OF* experiments) to derive a new parametrization and, eventually, a new overtopping predictive model. Indeed, we introduced dimensionless variables that account for the main parameter required to properly describe the overtopping process in shallow water (e.g., the new variable $\zeta_{1/4}$, the deep water peak period, and the foreshore slope). Almost 200 laboratory tests corroborated the good explanatory power of our parametrization and allowed us to provide a new overtopping model (Eq. 8). The latter can be used for seawalls with shallow, very and extremely shallow foreshores; indeed, it is valid for both breaking and non-breaking waves.

REFERENCES

Altomare, C., Gironella, X., and A.J. Crespo. 2021. Simulation of random wave overtopping by a WCSPH model. *Applied Ocean Research,* 116, 102888

Buccino, M., Di Leo, A., Tuozzo, S., Lopez, L.F.C., Calabrese, M., and F. Dentale. 2023. Wave overtopping of a vertical seawall in a surf zone: a joint analysis of numerical and laboratory data. *Ocean Engineering,* 288, 116144.

Buccino, M., Daliri, M., Buttarazzi, M. N., Del Giudice, G., Calabrese, M., and R. Somma. 2022. Arsenic contamination at the Bagnoli Bay seabed (South Italy) via particle tracking numerical modeling: Pollution patterns from stationary climatic forcings. *Chemosphere*, 303, 134955.

Buccino, M., Daliri, M., Calabrese, M., and R. Somma. 2021. A numerical study of arsenic contamination at the Bagnoli bay seabed by a semi-anthropogenic source. Analysis of current regime. *Science of the Total Environment*, 78215, 146811.

Calabrese, M., and M. Buccino. 2000. Wave impacts on vertical and composite breakwaters. In *Proceedings of the 10th International Ocean and Polar Engineering Conference*, Seattle.

Lopez, L. F. C., D. Salerno, F. Dentale, A. Capobianco, and M. Buccino. 2016. Wave overtopping at Malecòn tradicional, La Habana, Cuba. *Coastal Engineering Proceedings*, Antalya, Turkey, 17-20 November 2016, pp.24-24.

den Bieman, J.P., van Gent, M.R., and H.F. van den Boogaard. 2021. Wave overtopping predictions using an advanced machine learning technique. *Coastal Engineering*, 166, 103830

Di Leo, A., Dentale, F., Buccino, M., Tuozzo, S., and E. Pugliese Carratelli. 2022. Numerical analysis of wind effect on wave overtopping on a vertical seawall. *Water*. 14(23), 3891.

Etemad-Shahidi, A., Koosheh, A., and M.R. van Gent. 2022. On the mean overtopping rate of rubble mound structures. Coast. Eng. 177, 104150

EurOtop, Van der Meer, J.W., Allsop, N.W.H., Bruce, T., De Rouck, J., Kortenhaus, A., and T. Pullen. 2018. Manual on Wave Overtopping of Sea Defences and Related Structures. An overtopping Manual Largely Based On European research, but for Worldwide Application. Schüttrumpf.

Hedges, T.S., and M.T. Reis. 1998. Random wave overtopping of simple seawalls: a new regression model. Water Maritime Energy Journal, ICE 130, 1–10.

Hofland, B., Chen, X., Altomare, C., and P. Oosterlo. 2017. Prediction formula for the spectral wave period Tm-1,0 on mildly sloping shallow foreshores. *Coastal Engineering*, 123, 21–28

Kamphuis, J. W. 1991. Incipient wave breaking. *Coastal Engineering*, 15(3), 185-203.

Lam, D.C.L., and R.B. Simpson. 1976. Centered differencing and the box scheme for diffusion convection problems. *Journal of Computational Physics*, 220 (4), 486–500.

Lashley, C.H., Brown, J.M., Yelland, M.J., Van der Meer, J.W., and T. Pullen. 2023. Comparison of deep-water-parameter-based wave overtopping with wirewall field measurements and social media reports at Crosby (UK). *Coastal Engineering*, 179, 104241

Lashley, C.H., van der Meer, J.W., Bricker, J.D., Altomare, C., Suzuki, T., and K. Hirayama. 2021. Formulating wave overtopping at vertical and sloping structures with shallow foreshores using deep-water wave characteristics. *Journal Waterway Port Coastal Ocean Engineering*, 147, 6.

Losada, I.J., Lara, J.L., Guanche, R., and J.M. Gonzalez-Ondina. 2008. Numerical analysis of wave overtopping of rubble mound breakwaters. *Coastal Engineering*, 55 (1), 47–62.

Owen, M.W. 1980. Design of seawalls allowing for wave overtopping. Hydraulics Research. Wallingford, Report No. EX 924, UK.

Rijnsdorp, D.P., Smit, P.B., and M. Zijlema. 2014. Non-hydrostatic modelling of infragravity waves under laboratory conditions. *Coastal Engineering*, 85, 30–42.

Romano, A., Bellotti, G., Briganti, R., and L. Franco. 2015. Uncertainties in the physical modelling of the wave overtopping over a rubble mound breakwater: the role of the seeding number and of the test duration. *Coastal Engineering*, 103, 15–21.

Smit, P., Zijlema, M., and G. Stelling. 2013. Depth-induced wave breaking in a nonhydrostatic, near-shore wave model. *Coastal Engineering*, 76, 1–16.

Suzuki, T., Altomare, C., Veale, W., Verwaest, T., Trouw, K., Troch, P., and M. Zijlema. 2017. Efficient and robust wave overtopping estimation for impermeable coastal structures in shallow foreshores using SWASH. *Coastal Engineering*, 122, 108–123.

Tuozzo, S., Calabrese, M., and M. Buccino. 2024. An overtopping formula for shallow water vertical seawalls by SWASH. *Applied Ocean Research*, 148, 104009.

Vicinanza, D., Dentale, F., Salerno, D., and M. Buccino. 2015. Structural response of seawave Slot-Cone Generator (SSG) from Random Wave CFD simulations. In *Proceeding of the 25th International Ocean and Polar Engineering Conference,* Kona, Big Island.

Yuhi, M., Mase, H. Kim, S., Umeda, S., and C. Altomare. 2021. Refinement of integrated formula of wave overtopping and runup modeling. *Ocean Engineering*, 220: 108350.

Zanuttigh, B., Formentin, S., and J.W. Van der Meer. 2016. Prediction of extreme and tolerable wave overtopping discharges through an advanced neural network. *Ocean Engineering*, 127, 722.

Zijlema, M., Stelling, G., and P. Smit. 2011. SWASH: an operational public domain code for simulating wave fields and rapidly varied flows in coastal waters. *Coastal Engineering*, 58 (10), 992–1012